Phase State of Polyelectrolyte Complexes Based on Blends of Acrylic Copolymers

T. I. Kiseleva,[1] G. A. Shandryuk,[1] R. R. Khasbiullin,[2] A. A. Shcherbina,[2] A. E. Chalykh,[2] M. M. Feldstein[1,3]*

[1]*A. V. Topchiev Institute of Petrochemical Synthesis, Russian Academy of Sciences, 29, Leninsky Prospect, 119991, Moscow, Russia*
[2]*A. N. Frumkin Institute of Physical Chemistry and Electrochemistry, Russian Academy of Sciences, 31, Leninsky Prospect, 119991, Moscow, Russia*
[3]*D. I. Mendeleev University of Chemical Technology of Russia, 9, Miusskaya sqr., 125047, Moscow, Russia*

Received 4 April 2010; accepted 16 December 2010
DOI 10.1002/app.34044
Published online 6 July 2011 in Wiley Online Library (wileyonlinelibrary.com).

ABSTRACT: The phase state of polyelectrolyte blends based on acrylic copolymers was investigated with differential scanning calorimetry, transmission electron microscopy (TEM), and wedge microinterferometry as a function of the blend composition and ionization of polymer functional groups. A copolymer of *N*,*N*-dimethylaminoethyl methacrylate with methyl methacrylate and butyl methacrylate was used as a polybase, a copolymer of methacrylic acid and ethyl acrylate was employed as a polyacid, and the optional plasticizer was triethyl citrate. A correlation was established between an earlier described mechanism of molecular interaction and the behavior of the glass-transition temperature (T_g) of the polymer blends. The T_g values of the polyelectrolyte complexes in the gel phase were always higher than T_g in the sol phase. This fact implies that intermolecular cohesion dominated the free volume in the stoichiometric polyelectrolyte complexes formed in the gel phase, whereas nonstoichiometric complexes formed in the sol phase were characterized with the predominant contribution of free volume. TEM and interferograms of polyelectrolyte blends showed the signs of anisotropic ordered supramolecular structure formation. A phase-state diagram of the polyelectrolyte blends was constructed. The stoichiometric polyelectrolyte complex was immiscible with parent polymers, forming a separate phase that became melted at elevation of temperature because of complex dissociation. Polyelectrolyte miscibility was supposed to result rather from the chemical reaction of the complex formation than from interdiffusion of the polymer components along the gradient of their concentration. © 2011 Wiley Periodicals, Inc. J Appl Polym Sci 122: 2926–2943, 2011

Key words: cooperative effects; phase behavior; polyelectrolytes; polymer blends; solid-state structure

INTRODUCTION

The phase state and physical properties of polymer materials are functions of their chemical structure.[1–3] If a quantitative structure–property relationship (QSPR) is explored, a number of fundamental physical characteristics of polymers may be predicted from their chemical structure.[4,5] Numerous correlations have been reported in the literature between the chemical structure of polymers[6–8] and the mechanisms of their molecular interactions in blends[9] on the one hand, and the phase state of polymer composites on the other. In turn, on a macroscopic scale, the physical properties of polymer materials are governed by their phase state and, consequently, by their molecular structure.[10–15]

From a practical point of view, knowledge of QSPR is of considerable importance for the rational design of new materials with tailored performance properties. The final goal of our research was the molecular design of new pressure-sensitive adhesives (PSAs), produced by the blending of nonadhesive polymers. PSAs are viscoelastic polymer materials capable of forming strong adhesive bonds with substrates of various chemical natures under the application of a slight pressure (1–10 Pa) over a short period of time (1–2 s).[16] On a molecular level, pressure-sensitive adhesion is the result of a specific balance between the high energy of intermolecular cohesion and a large free volume.[17,18] Hence, to develop PSAs, rationally we should identify the molecular structures that meet these usually conflicting requirements.

As recent investigations in our group have shown, the mechanisms of formation of interpolymer and

**Present address:* A.V. Nesmeyanov Institute of Organoelement Compounds, Russian Academy of Sciences, 28, Vavilova str., 119991, Moscow, Russia.

Correspondence to: T. I. Kiseleva (kiseleva@ips.ac.ru) or M. M. Feldstein (mfeld@ips.ac.ru).

Contract grant sponsor: Corium International, Inc., Menlo Park, CA, and U. S. Civilian Research & Development Foundation; contract grant number: RUC1-1658-MO-06.

polymer–oligomer complexes can underlie the molecular design of new PSAs prepared by the blending of nonadhesive polymers and oligomers.[19,20] In polymer blends involving the formation of polyelectrolyte complexes between the macromolecules of a polybase and a polyacid, a high cohesion strength is provided by hydrogen, electrostatic, or ionic bonding between macromolecules carrying complementary groups in their main chains, whereas a large free volume can result from the occurrence of loops and other defects of a supramolecular network structure. Although the mechanisms of molecular interactions in the binary and ternary blends of a polybase and polyacid with and without appropriate plasticizer have been considered in a recent article by our group,[21] in this second article of the series, we focus on the phase state of polyelectrolyte blends involving polybase–polyacid complex formation. The adhesive, mechanical, and other performance properties of the PSA based on interpolymer complexes will be the subject of following publications.

Although a considerable amount of research work has been performed on the formation and properties of interpolymer complexes in solutions,[22–32] there is a lack of experimental data on the phase behavior of oppositely charged polyelectrolyte blends in a solid state. Using Fourier transform spectroscopy and differential scanning calorimetry (DSC), we recently studied the impact of competitive hydrogen bonding on the phase behavior in the triple blends of poly(*N*-vinyl pyrrolidone) with oligomeric poly(ethylene glycol) (PEG) and a copolymer of methacrylic acid (PMAA) with ethyl acrylate (EA).[33] The obtained results allowed us to gain a molecular insight into viscoelastic behavior and adhesion of the poly(*N*-vinyl pyrrolidone)–PEG–PMAA-*co*-EA blends.[34,35] In this study we applied this earlier developed approach to elicit a relationship between the phase state and molecular interactions in the blend of a polybase [a copolymer of poly(*N*,*N*-dimethylaminoethyl methacrylate) (PDMAEMA) with methyl methacrylate (MMA) and butyl methacrylate (BMA)], a polyacid (PMAA-*co*-EA), and a plasticizer [triethyl citrate (TEC)].

The phase state of polymer blends is so closely allied to molecular interactions that in some instances, the amount of hydrogen bonds formed between blend components can be evaluated from the compositional behavior of the glass-transition temperature (T_g).[36–38] The thermodynamic parameters of pair interactions can be calculated from the phase diagrams of polymer blends.[23,39] In this connection, it is quite pertinent to consider the phase state of polymeric systems as a function of the molecular interactions between the functional groups of macromolecules in the blend. On the basis of the gained insight into the energetic and geometrical characteristics of interpolymer bonds in PDMAEMA-*co*-MMA/BMA – PMAA-*co*-EA blends with and without TEC plasticizer, which were reported in our previous publication,[21] we draw now our attention to the phase behavior of these blends. Thus, this article partly fills a gap in information about the phase behavior of polyelectrolyte complexes in the solid state.

EXPERIMENTAL

Materials

As a polybase, in this work, we used the copolymer of *N*,*N*-dimethylaminoethyl methacrylate (DMAEMA) with MMA and BMA (PDMAEMA-*co*-MMA/BMA, molar ratio = 2 : 1 : 1, molecular weight $\sim$ 150,000 g/mol). The polybase was commercially available from Röhm Pharma GmbH (Darmstadt, Germany) as Eudragit E-100. As a polyacid, we employed PMAA-*co*-EA (molar ratio = 1 : 1, molecular weight $\approx$ 250,000 g/mol), which was obtained as Eudragit L-100-55 from Evonik Degussa Corp. (Piscataway, NJ), subsidiary of Evonik Röhm GmbH, Germany. Both polymers were used as received.

The preparation of polyelectrolytes charged to a predetermined degree of ionization of ionogenic groups was provided by the treatment of their water–alcohol (50 : 50) solutions by aqueous solutions of HCl (for polybase ionization) or NaOH (for ionization of the polyacid). With this purpose, the amounts of HCl or NaOH required for full ionization of the ionogenic groups was measured in advance with potentiometric titration. The degrees of polyelectrolyte ionization of 10 and 50% corresponded to 0.1 and 0.5, respectively, of the gram equivalents of the HCl and NaOH required for full ionization of the polyelectrolyte.

According to potentiometric titration data, the initial PDMAEMA-*co*-MMA/BMA copolymer contained no protonated amino groups. At the same time, the degree of dissociation of the carboxyl groups in the initial PMAA-*co*-EA polyacid was 2.5–3%.

The plasticizer for this work was TEC (obtained from Morflex, Inc., Greensboro, NC). The molecular structures of the materials employed in our research are shown in Figure 1.

Preparation of the experimental samples

The films of polybase–polyacid blends with and without plasticizer were prepared by a casting–drying method from ethanol solutions. The required amount of polybase was first dissolved in ethanol under vigorous stirring (600–700 rpm) with a Cole–Parmer laboratory mixer (model 50002-25) (Vernon

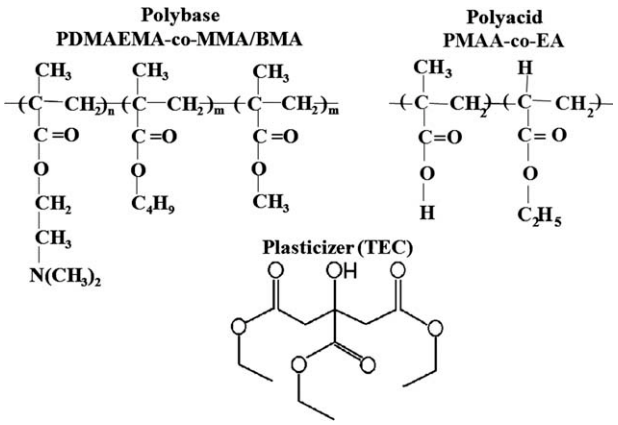

Figure 1 Molecular structures of PDMAEMA-*co*-MMA/BMA, PMAA-*co*-EA, and TEC.

Hills, Illinois). The stirring rate was then increased to 900–1000 rpm, and the PMAA-*co*-EA polyacid was slowly added. This mixture was then kept stirring for 16 h until a homogeneous solution was obtained. The TEC plasticizer was added to the polymer solution under stirring with a magnetic stirrer. The total concentration of polymers in ethanol averaged 38–40 wt %. As a rule, solutions containing 20 : 1 and 10 : 1 polybase–polyacid weight ratios were clear, whereas the blends with higher PMAA-*co*-EA concentrations were opaque. In some particular cases, the inhomogeneous solutions of 5 : 1, 2 : 1, and 1 : 1 polybase–polyacid weight ratios were filtered for the separation of a sediment (gel fraction) from a supernatant phase (sol fraction). The prepared solutions were then cast onto a poly(ethylene terephthalate) casting sheet (PEBAX-600) (Philadelphia, PA). A uniform thickness of the films was obtained with a BYK-Gardner film casting knife (AG-4300 series) (Columbia, MD), as described earlier.[39] The wet film thickness was 0.5 mm, and the thickness of the dry film was 80–100 μm. The films were dried overnight at ambient conditions (19–22°C). Upon drying, the films were covered by a second sheet of the PEBAX-600 release liner.

RESEARCH METHODS

Potentiometric titration was performed on Ecotest-120 pH meter (obtained from Econix, Ltd., Moscow, Russia). For determination of the gram equivalents of the HCl and NaOH needed for complete ionization of polyelectrolytes, the polyelectrolyte analyte was first dissolved in a 1 : 1 mixture of ethyl alcohol with distilled water, and the obtained 1% solution was then titrated by 0.2*N* HCl or 0.1*N* NaOH aqueous solutions. The titration curves had a characteristic sigmoidal shape. The section of the curve that demonstrated the maximum pH change marked the equivalence point of the titration.

DSC was used to characterize the phase state of the polyelectrolytes and their blends. In the DSC apparatus, the samples were first quench-cooled with liquid nitrogen from ambient temperature to −150°C, subjected to isothermal annealing at this temperature, and then heated up to 220°C at a rate of 20°C/min. The DSC heating traces were measured with a Mettler TA 4000/DSC 30 thermoanalyzer, calibrated with indium and gallium. In the DSC measurements, the samples of 5–15 mg in weight were sealed in standard aluminum pans supplied with pierced lids so that absorbed moisture could evaporate upon heating. An argon purge (50 mL/min) was used to prevent moisture condensation at the sensor. All reported values of the DSC thermograms are the average of replicate experiments varying less than 1–2%.

The determination of absorbed water amounts in the blends was done gravimetrically by the termination of weight loss upon drying *in vacuo*. In addition, we also measured the content of water by weighing the samples before and after DSC scans using a Mettler analytical (Columbus, OH) balance (E 240) with an accuracy of ±0.01 mg. The weight loss of the sample after scanning was compared to the amount of desorbed water evaluated from the enthalpy change associated with water evaporation from the sample by DSC.

Wide-angle X-ray diffraction measurements (WAXS) were performed with Cu Kα radiation with a DRON-2 diffractometer (St. Petersburg, Russia) with an asymmetric focusing curved quartz crystal monochromator of a primary beam equipped with a thermocontrolled camera. The diffraction patterns were recorded in reflectance mode. The scattering intensity distribution was measured with a step-scanning device at a step interval of 0.02°, with the range of twice the Bragg angles from 1 to 50°.

Wedge microinterferometry (WMI) was used to study the miscibility of the blend components, as reported earlier.[35,40,41] The custom-made WMI cell consisted of two mirrors formed by finely polished glass slides that were coated on one side with nickel alloy, which permitted 40% light transmittance. The mirrors faced each other and were separated by two parallel metal bars of thicknesses 80 μm and 100 μm, spaced 2 cm apart and forming a wedged gap with a wedge angle of 0.001 rad. A film sample 5 mm long and 1 mm wide was loaded into the apparatus cell with the mirrors left loose. The sample was heated in the cell at 175°C over 30 min to ensure good optical contact of the mirrors with the sample. The system was then cooled to a temperature of measuring and equilibrated at this temperature for 30 min. The heating cycle did not irreversibly affect the properties of blends because all of the components of the blends were stable within this temperature range.

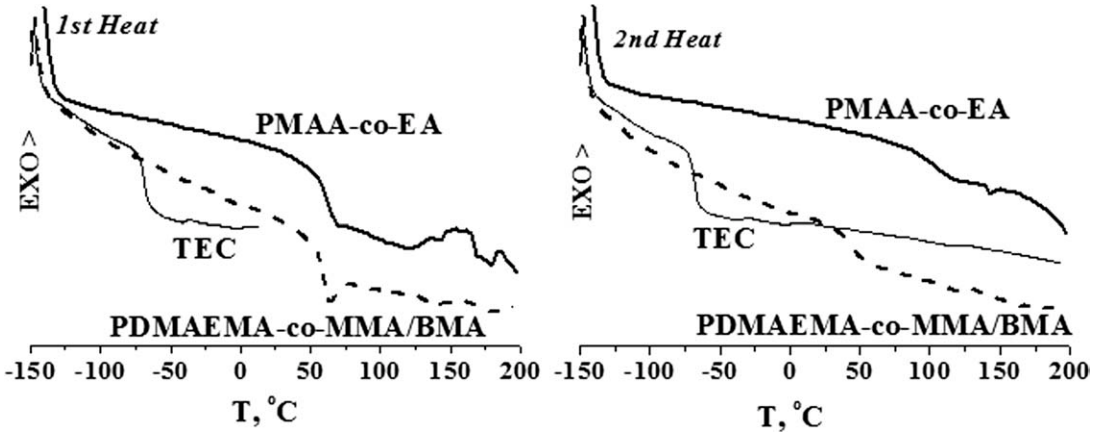

Figure 2 DSC thermograms under the first and repeated heating of the unblended PDMAEMA-*co*-MMA/BMA polybase, PMAA-*co*-EA polyacid, and TEC plasticizer (T = temperature).

The cell was mounted horizontally and illuminated from below by a helium–neon laser beam with a wavelength of 633 nm. The film of other solid polymer or a drop of liquid TEC was introduced into the cell, filling the gap between the mirrors and making contact with one of the film's edges. Interference patterns were observed through an optical microscope at different magnifications, ranging from 60- to 160-fold, with the objective placed over the film–solution interface. Photographs were captured with a black-and-white video camera at specified time points, and fringe densities were converted to concentration profiles by methods described elsewhere.[40,42]

Transmission electron microscopy (TEM) studies were performed with a Philips EM-301 microscope (Philips Research High Tech Campus 55656 AE Eindhoven The Netherlands) under 10^4 to 10^5 magnification. Two groups of specimens were prepared. The first group was represented by interfacial contact zones, obtained by joint pressing and thermal annealing at 170°C of the two laminated films. The second group was the films of the 30 : 70 (wt %) blends, prepared by casting from ethyl acetate solution onto the surface of mica. For structural investigation, the surfaces of the samples were etched with HF plasma oxygen discharge at 0.03 Torr, 10 MHz of frequency, and 4–6 eV of electron energy. A single-stage C—Pt replica of the etched surface was scanned on an electron microscope.

RESULTS AND DISCUSSION

DSC characterization of the phase behavior in the polybase–polyacid–plasticizer blends

Phase state of the unblended components

During the first heating, the DSC thermogram of the initial PMAA-*co*-EA (Fig. 2, Table I) exhibited a T_g of 59.4°C [a change of heat capacity at glass transition (ΔC_p) = 0.63 J g^{-1} K^{-1}] and signs of the polymer decomposition at temperatures above 120°C. ΔC_p is useful demonstrative indicator as the glass transition is pronounced. In the second heating, the glass transition shifted to 104.8°C (ΔC_p = 0.36 J g^{-1} K^{-1}); however, because of the partial decomposition of this sample in the course of the first heating, the results of repeated scanning could not be taken into further consideration. As 20% of the carboxyl groups of PMAA-*co*-EA were ionized by the treatment with NaOH solution, T_g in the first scan increased (T_g = 64.1°C, ΔC_p = 0.83 J g^{-1} K^{-1}, Fig. 2 and Table I), whereas the thermal decomposition of the polymer occurred at temperatures above 140°C). The PMAA-*co*-EA copolymer with 50% ionized carboxyl groups demonstrated a very broad glass transition that could be characterized with two T_g's at 52.3°C (ΔC_p = 0.67 J g^{-1} K^{-1}) and 87.7°C (ΔC_p = 0.57 J g^{-1} K^{-1}), respectively. Such a wide glass transition was indicative of the phase inhomogeneity of the partly neutralized polyacid.

Although the earlier described DSC heating thermograms of nonionized and partly ionized PMAA-*co*-EA exhibited no absorbed water in the sample, the fully ionized sodium salt of the polyacid contained 11.9 wt % water (Fig. 2). Against a background of a broad symmetric water evaporation endotherm with a peak at 115.6°C, the glass transition could not be detected. Repeated heating up to 200°C of the sample dried in the course of the first scanning revealed no glass transition and no evidences of polymer decomposition. As long as the sodium PMAA-*co*-EA salt was thermally stable, a third scanning was made, which showed T_g at 50.5°C (ΔC_p = 0.56 J g^{-1} K^{-1}, Table I).

The initial PDMAEMA-*co*-MMA/BMA polybase was supplied in the form of granules. As follows from the DSC curves presented in Figure 2, it had a T_g of 58.3°C (ΔC_p = 0.48 J g^{-1} K^{-1}) and exhibited no

TABLE I
T_g's and the Values of ΔC_p for the Initial Polyelectrolytes and the Effect of Functional Group Ionization on the Glass Transition

Polyelectrolyte	Ionized groups (mol %)	Water content (wt %)		T_g (°C)		ΔC_p (J g^{-1}·K^{-1})	
		First scan	Second scan	First scan	Second scan	First scan	Second scan
PMAA-*co*-EA	0	0	0	59.	104.8	0.63	0.36
	20	0	0	4	42.5	0.83	0.73
	50	0	—	64.1	—	0.67	–
	100	11.9	0	52.3 ?	–/50.5[a]	–	–/0.56[a]
PDMAEMA-*co*-MMA/BMA	0	0	0	57.	44.2	0.32	0.26
	20	3.5	0	6	56.5	0.45	0.16
	50	7.0	0	58.	91.4	0.43	0.57
	100	8.3	0	1 59.6 ?	125.9	?	0.34

[a] Third heating.

evidences of thermal decomposition under heating up to 200°C. Uncharged PDMAEMA-*co*-MMA/BMA contained no absorbed water. Under repeated scanning, the polybase demonstrated a lower T_g value (43.3°C, $\Delta C_p = 0.24$ J g^{-1} K^{-1}, Fig. 2). Similar T_g's were established for the PDMAEMA-*co*-MMA/BMA film obtained by casting and drying from an ethyl alcohol solution: 57.6°C ($\Delta C_p = 0.32$ J g^{-1} K^{-1}) and 44.2°C ($\Delta C_p = 0.26$ J g^{-1} K^{-1}) under the first and second scannings, respectively (Table I). As 20 mol % of the DMAEMA recurring units were protonated by the treatment of polymer with HCl aqueous solution, the polybase contained 3.5–4.4 wt % of absorbed water. In the course of the first scanning, a wide endotherm of water evaporation at 100°C obscured the glass transition, which became observable only in the thermogram of repeated heating (T_g = 56.5°C, $\Delta C_p = 0.16$ J g^{-1} K^{-1}; DSC thermograms are not presented). If PDMAEMA-*co*-MMA/BMA amino groups were protonated by 50 mol %, the water sorption increased twice as much (7.0 wt %). The glass transition became apparent as a shoulder on the peak of water thermodesorption (T_g = 59.6°C, $\Delta C_p = 0.43$ J g^{-1} K^{-1}); however, the evaluated values were not reliable. The second heating of the sample dried under previous scanning demonstrated highly wide glass transitions between 55.2 and 119.8°C, T_g = 119.8°C, and $\Delta C_p = 0.57$ J g^{-1} K^{-1}. Complete protonation of PDMAEMA-*co*-MMA/BMA amino groups (by 100 mol %) resulted in a further rise of water absorption (8.3 wt %), which makes the glass transition undetectable in the first scanning. Repeated scans displayed rather a narrow glass transition at T_g = 125.9°C and $\Delta C_p = 0.34$ J g^{-1} K^{-1} (Table I).

The DSC thermogram of the unblended TEC plasticizer (Fig. 2) showed T_g at −68.8°C ($\Delta C_p = 0.65$ J g^{-1} K^{-1}) and no signs of evaporation or thermal decomposition at heating up to 200°C. Under repeated heating, this T_g value remained unchanged (−68.4°C).

Relation of T_g to mechanisms of molecular interaction

It is known that T_g relates to the energy of cohesion and free volume (vacant space between neighboring macromolecules) by the following equation:[2]

$$T_g = 0.455 \frac{z\langle D_o \rangle}{R} \quad (1)$$

where R is the gas constant; z is the coordination number, a value that is inversely proportional to the free volume; and $\langle D_o \rangle$ is the total intermolecular cohesion energy. The ionization of PMAA-*co*-EA carboxyl groups affects both the energy of intermolecular cohesion and the free volume governing the T_g behavior. As has been shown earlier,[21,33] all of the carboxyl groups in the PMAA-*co*-EA polyacid were self-associated through hydrogen bonding, and the interaction energy of the uncharged carboxyl group was 26.5 kJ/mol. Partial ionization of the carboxyl groups and the appearance of carboxylate anions led to the hydrogen complex formation between the uncharged and charged carboxyl groups. Such a complex was much more energetically favorable (the complexation energy ranges from 73.5 to 89.9 kJ/mol).[21] In accordance with Eq. (1), it was logically to suppose that the increase in the the cohesion energy due to partial ionization of the carboxyl groups may have resulted in the increase of the T_g value. On the other hand, electrostatic repulsion of the negatively charged carboxylate anions could have caused the increase of free volume that decreased both the z and T_g values. The observed impact of the carboxyl group ionization on the glass transition in the partly charged PMAA-*co*-EA polyacid was the result of both of these contributions. The occurrence of two distinct T_g values in the DSC scan of the partly ionized PMAA-*co*-EA could be explained by the coexistence of uncharged carboxyl groups, their self-associates, free carboxylate anions, and H-bonded complexes with the uncharged carboxyl groups.

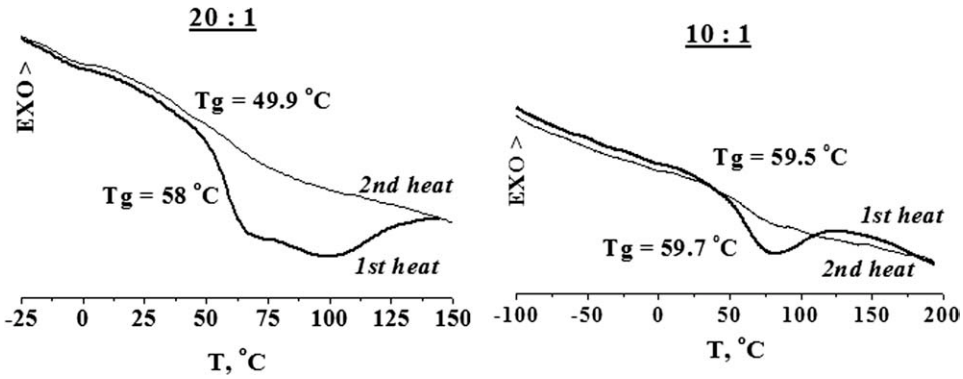

Figure 3 DSC thermograms of the PDMAEMA-*co*-MM/BMA blends with PMAA-*co*-EA under the first and repeated heating. The polybase–polyacid weight ratios were 20 : 1 (left) and 10 : 1 (right; T = temperature).

As follows from the DSC data shown in Table I, the protonation of PDMAEMA amino groups led to a remarkable increase in the polybase T_g from 44.2 to 125.9°C; this implied a predominate effect of the rise of intermolecular cohesion energy over the increase of free volume. This fact became comprehensible once we took into account the mechanisms of molecular interaction between the amino and ammonium functional groups in the PDMAEMA polycation, considered in a recent article of our research group.[21] As was shown in this article, the strength of interaction increased in a row: the associate of an ammonium cation with an uncharged amino group (46.77 kJ/mol) $\ll$ a complex of an uncharged amino group with an ammonium cation tightened by a chlorine counterion (421.02 kJ/mol) $<$ a dimeric complex of two ammonium cations with a chlorine counterion (666.48 kJ/mol).

In such a way, the ionization of recurring functional groups of polyelectrolytes and the mechanism of their bonding appreciably affected the phase behavior of the unblended polymer components.

Phase state of the binary polybase–polyacid blends

Figure 3 illustrates DSC thermograms of the binary PDMAEMA-*co*-MMA/BMA polybase blends with comparatively small amounts of PMAA-*co*-EA polyacid. Within this range of blend compositions, the DSC thermograms exhibited only a single T_g, which was close to the T_g values of both of the unblended polymers. Thus, in the first scan, the T_g's of the polybase–polyacid blends taken in weight ratios of 20 : 1 and 10 : 1 were, correspondingly, 58.8 and 59.5°C (ΔC_p = 0.47 and 0.59 J g^{-1} K^{-1}, respectively). At repeated scanning, T_g of the 20 : 1 blend became lower (T_g = 49.9°C, ΔC_p = 0.29 J g^{-1} K^{-1}), whereas T_g of the 10 : 1 blend remained unaffected (T_g = 59.7°C, ΔC_p = 0.25 J g^{-1} K^{-1}). Although absorbed water is a good plasticizer for polyelectrolyte blends, nevertheless, its content in the PDMAEMA-*co*-MMA/BMA – PMAA-*co*-EA blends was negligible (<0.5 wt %) for a pronounced plasticization effect.

Effect of the TEC plasticizer on the phase behavior of the polybase–polyacid blends

Being miscible with polymer components and possessing a very low value of T_g (−68.8°C), TEC was a good plasticizer for the PDMAEMA-*co*-MMA/BMA polybase–PMAA-*co*-EA polyacid blends. As follows from the data presented in Figures 4 and 5, the T_g value decreased smoothly with the increase of TEC concentration in the blends. The occurrence of two distinct T_g's was observed only for the 10 : 1 polybase–polyacid blend with 25 wt % TEC plasticizer under repeated heating (T_g = −21.3 and 114.3°C, ΔC_p = 0.26 and 0.13 J g^{-1} K^{-1}), which was dried in the course of the first heating (Fig. 4). The hydrated blend, containing 0.5 wt % absorbed water, and all of other blends displayed only a single glass transition. In this way, the addition of appropriate plasticizers promoted the formation of homogeneous blends, whereas the increase of the content of noncovalent crosslinker, PMAA-*co*-EA, led to the separation of the polyelectrolyte complex into individual phases.

As is evident from the DSC data presented in Figure 6, the T_g values measured in the course of the first and repeated scanning were very close. This conclusion was explainable because the content of absorbed water in the samples did not exceed 0.5 wt %. Interestingly, the dry 20 : 1 polybase–polyacid blends containing comparatively small amounts of TEC plasticizer exhibited lower T_g values than the hydrated blends (Fig. 6, left). Taking into account that water has a very low T_g value and serves as a good plasticizer for polyelectrolyte complexes, we expected the lower T_g magnitudes for the wet blends. The implication of this fact became

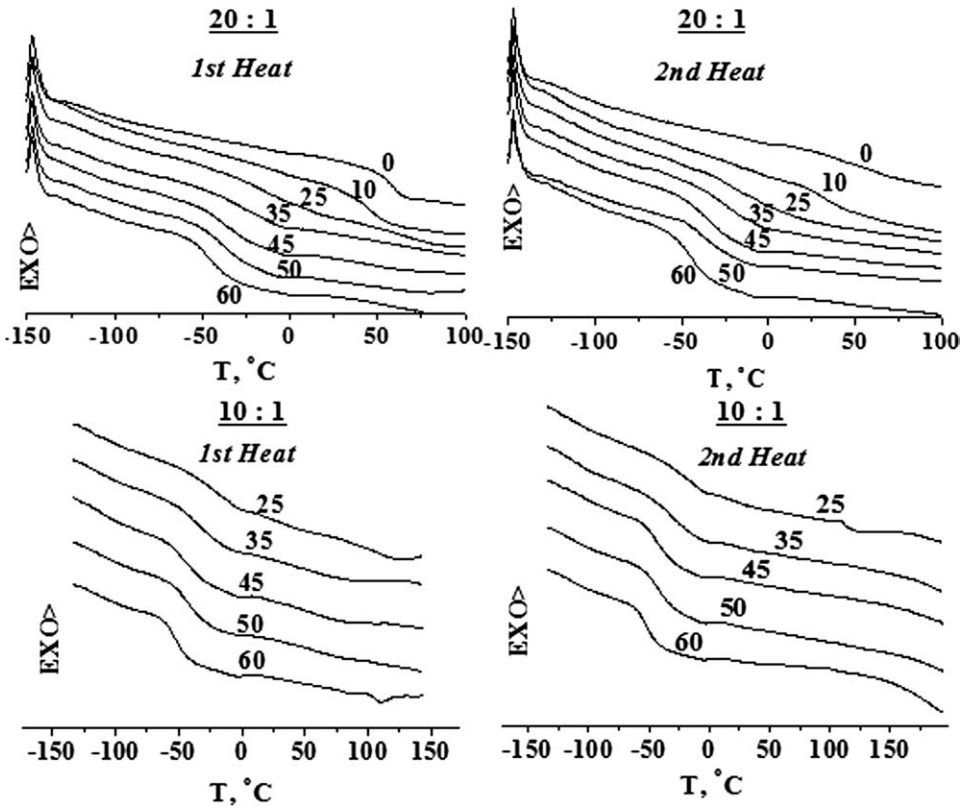

Figure 4 Effect of the TEC concentration on the DSC thermograms of the PDMAEMA-*co*-MM/BMA blends with PMAA-*co*-EA under the first and repeated heating. The polybase–polyacid weight ratios were 20 : 1 (top) and 10 : 1 (bottom; T = temperature).

understandable when we took into consideration the strong interaction of water molecules with functional groups in the PDMAEMA-*co*-MMA/BMA and PMAA-*co*-EA macromolecules in the blends, which was described in our recent article.[21] As was established in this study, water forms comparatively weak H-bonded complexes with the DMAEMA amino group (energy of complex formation (ΔE) = 12.3 kJ/mol) and methacrylic acid carboxyl group (ΔE = 22.6 kJ/mol). This fact explains why PDMAEMA-*co*-MMA/BMA was drier than PMAA-*co*-EA. The energy of H-bonded complex formation between the amino and carboxyl groups was found to be 26.2 kJ/mol. At the same time, the energies of ternary H-bonded complexes formed by the amino and carboxyl groups involving water molecules were appreciably higher (ΔE = 37.9 and 42.9 kJ/mol). In the blends containing greater amounts of TEC plasticizer, the interaction of TEC with PDMAEMA-*co*-MMA/BMA (ΔE = 12.3 kJ/mol) and PMAA-*co*-EA (ΔE = 41.5 kJ/mol) should have also been taken into account. TEC complexes did not form stable hydrogen bonds with water molecules.[21] Thus, the data presented in Figure 6 imply that the contribution of a plasticization effect to the value of T_g may be obscured by the contribution of intermolecular interaction. In view of Eq. (1), it is clear that strong interaction increases the esnergy of intermolecular cohesion and, consequently, the T_g value.

Analysis of the compositional relationship of T_g

To gain an advanced insight into the mechanism of polymer mixing and interaction, it is often useful to compare the observed compositional relationship of

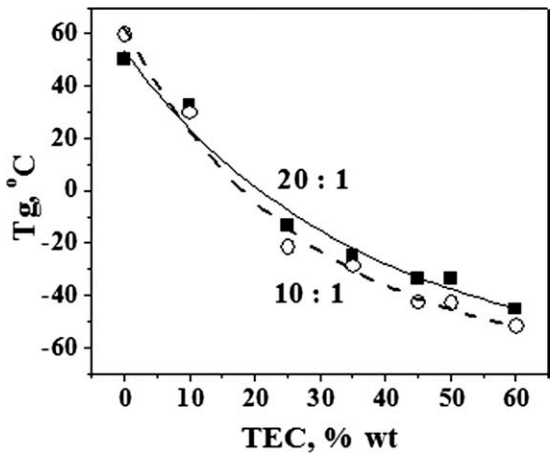

Figure 5 Effect of the TEC concentration on T_g of the PDMAEMA-*co*-MMA/BMA blends with PMAA-*co*-EA. The polybase–polyacid weight ratios were 20 : 1 and 10 : 1.

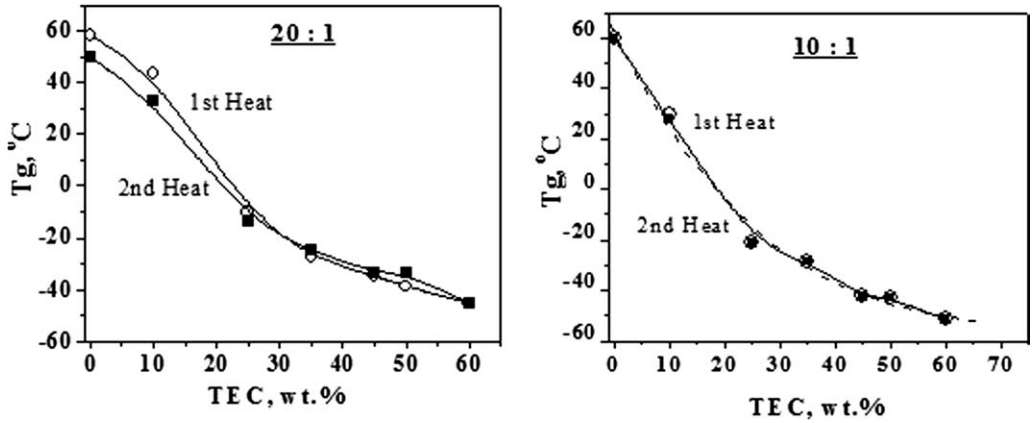

Figure 6 Comparison of the T_g values recorded in the course of the first and repeated heating for the polyelectrolyte blends with various amounts of TEC plasticizer.

T_g with the simple rule of mixing, expressed in the terms of the Fox or Gordon–Taylor equations.[43,44] Any deviations in the T_g behavior of a real polymer system from ideal dependence, described by the simple rule of mixing, is conventionally treated as a contribution of strong specific interaction between the polymer components.[36–38,45–52] In full agreement with Eq. (1),[2] negative T_g deviations are generally considered as a prevailing contribution of an excess volume formation under polymer–polymer or polymer–plasticizer mixing,[45–51] whereas positive T_g deviations have been reported for so-called ladder-like interpolymer complexes, wherein the increase of intermolecular cohesion energy is frequently accompanied with a decrease of free volume.[51,52]

Figure 7 compares the measured T_g dependence on the content of TEC plasticizer for 20 : 1 and 10 : 1 polybase–polyacid blends with an ideal behavior expressed in the terms of the Fox equation [Eq. (2)]:

$$\frac{1}{T_g} = \frac{w_{\text{polybase}}}{T_{g_{\text{polybase}}}} + \frac{w_{\text{polyacid}}}{T_{g_{\text{polyacid}}}} + \frac{w_{\text{plasticizer}}}{T_{g_{\text{plasticizer}}}} \qquad (2)$$

where w and T_g are the weight fractions and glass-transition temperatures of unblended PDMAEMA-*co*-MMA/BMA polybase, PMAA-*co*-EA polyacid, and TEC plasticizer. As is evident from the data in Figure 7, the points relating to the T_g values of non-plasticized polybase–polyacid blends displayed positive T_g deviations from the ideal relationship. The points referring to the ternary blends containing 10 wt % of the plasticizer exhibited ideal component mixing, whereas the points corresponding to the blends with greater amounts of the plasticizer demonstrated appreciable negative T_g deviations. The higher the content of PMAA-*co*-EA, the larger the deviations.

The implication of found deviations is that the polybase–polyacid system involved a strong interaction between both polymer components and the plasticizer. In the strict sense, the T_g's of the unblended polybase and polyacid could not be taken as reference values for the T_g calculation of their blends because the formation of strong hydrogen, electrostatic, or ionic bonds between their complementary functional groups affected their T_g values. Actually, as is shown previously, the introduction of

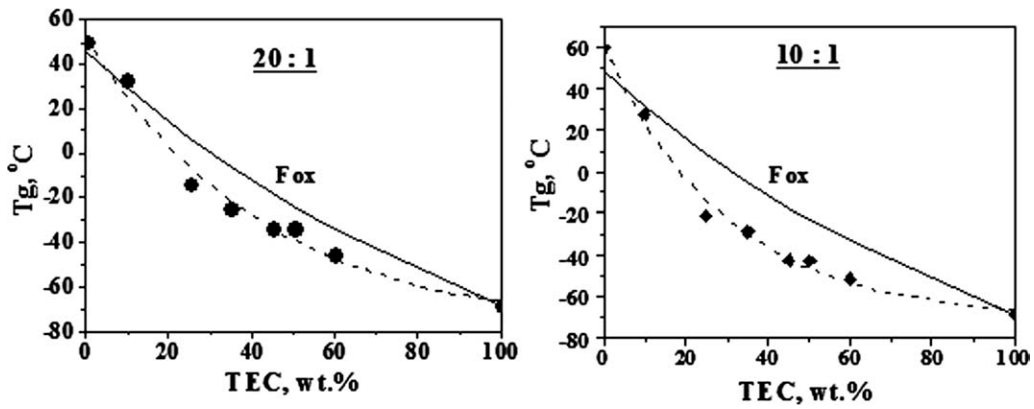

Figure 7 Effect of the TEC plasticizer on the T_g behavior in the PDMAEMA-*co*-MMA/BMA blends with PMAA-*co*-EA taken at weight ratios of 20 : 1 and 10 : 1 (the data of second scanning). The solid line represents the ideal relationship calculated with the Fox equation [Eq. (2)], and the points and dotted line are the measured T_g values.

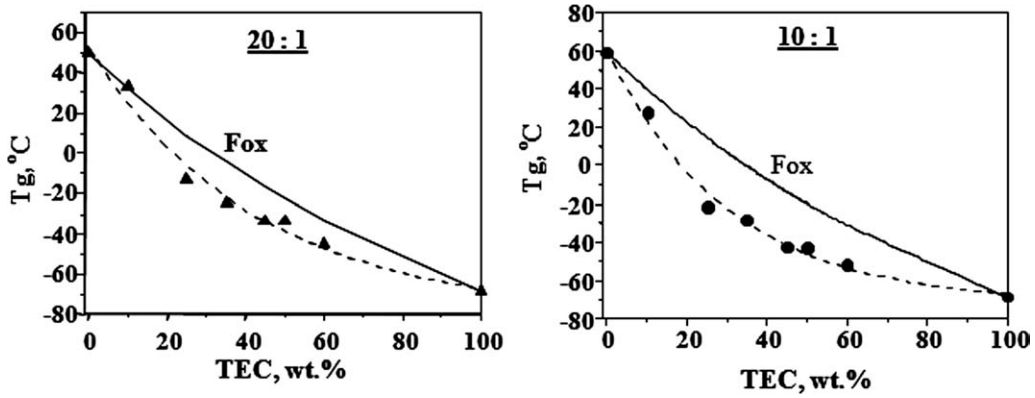

Figure 8 Impact of the TEC concentration on the T_g behavior in the PDMAEMA-*co*-MMA/BMA blends with PMAA-*co*-EA taken at weight ratios of 20 : 1 and 10 : 1 (the data of second scanning). The solid line represents the ideal relationship calculated with the Fox equation [Eq. (3)], and the points and dotted line relate to the measured T_g values.

ionized groups into polybase or polyacid chains led to an appreciable change of the T_g. As the data of quantum chemical calculations have shown,[21] in the PDMAEMA-*co*-MMA/BMA – PMAA-*co*-EA – TEC system, 35 structures of energetically favorable intermolecular complexes could be identified, including also the strong hydrogen-bonded complex with charge transfer. For this reason, to trace the impact of plasticizer on the T_g behavior in the polybase–polyacid blends, the use of T_g magnitude of the polyelectrolyte blend as a reference value was more appropriate than the use of the T_g of unblended polymer components.

To eliminate the impact of polybase–polyacid interaction from consideration and to explore the effect of TEC plasticizer only, Figure 8 shows the difference between T_g behaviors of our real PDMAEMA-*co*-MMA/BMA – PMAA-*co*-EA – TEC system and ideal mixing, described by the Fox equation in the following form:

$$\frac{1}{T_g} = \frac{w_{\text{polycomplex}}}{T_{g_{\text{polycomplex}}}} + \frac{w_{\text{plasticizer}}}{T_{g_{\text{plasticizer}}}} \tag{3}$$

where w and T_g are the weight fractions and glass-transition temperatures of the nonplasticized psolybase–polyacid complex and TEC plasticizer, correspondingly. In this case, only negative T_g deviations were observed, which were larger for the 10 : 1 system than for the 20 : 1 blend. The data presented in Figure 8 imply that the blend of the polybase–polyacid complex with TEC plasticizer could be treated as a solution of interpolymer complex in TEC, which was a good solvent for the PDMAEMA-*co*-MMA/BMA complex with PMAA-*co*-EA.

According to Eq. (1), positive T_g deviations signify the predominant contribution of the increase of intermolecular cohesion to the T_g magnitude. Negative T_g deviations are the evidence of the predominant contribution of an excess volume formation under component mixing, which in turn, is indicative of the formation of free volume. It is clear that generally, the cohesion and free volume are mutually contradicting material properties. If the cohesion is high enough, the free volume is usually small and vice versa. This brings up the question: because of what structure factors were the polyelectrolyte complexes capable of coupling the strong intermolecular cohesion with the large free volume?

The formation of interpolymer complexes proceeded according to the cooperative mechanism and led to the occurrence of long sequences of interchain bonds, which schematically resembled a ladder. Therefore, this type of complex is frequently referred to as a *ladderlike polycomplex*.[19,25,53,54] As schematically shown in Figure 9, in blends of complementary polymers including the formation of interpolymer complexes, a high energy of cohesion could be provided by the formation of intermolecular hydrogen, electrostatic, or ionic bonds and the crosslinking of the chains of the film-forming polymer into three-dimensional network structures. The cohesive strength of the network was controlled by the number and strength of interchain junctions. Two kinds of junctions may be distinguished. Junctions A represented the ladderlike sequences of interchain bonds, and their strength depended on the energy and amount of these bonds. Junctions B emerged via physical entanglements of long macromolecules in the blend. Their amount and strength were affected by the blend concentration and the length of the polymer chains. The free volume in the interpolymer complexes, along with other defects of the supramolecular network structure, could be produced by loops (C) of free macromolecular chains (Fig. 9). The size and amount of loops or the conversion of chemical reaction of the interpolymer complex formation in the solid phase were governed by the content and strength of polymer chain entanglements (B).

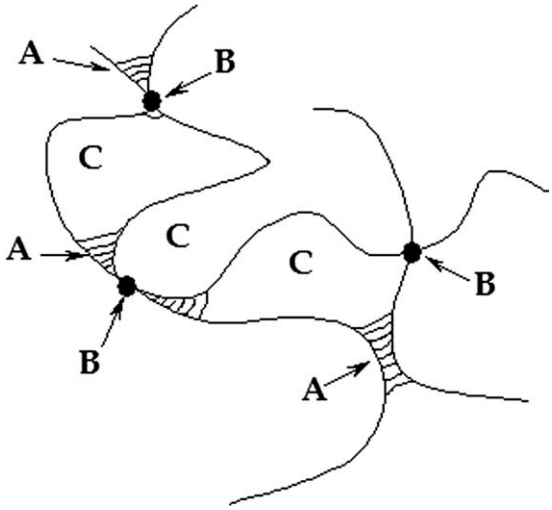

Figure 9 Schematic presentation of the noncovalently crosslinked network structure of the interpolymer complexes. (A) Noncovalent crosslinks consisting of sequences of hydrogen, electrostatic, or ionic bonds formed between functional groups in monomer units of complementary macromolecules. (B) Entanglement junctions of long polymer chains. (C) Loops consisting of the segments of macromolecules free of interpolymer bonding.

Effect of the polybase–polyacid ratio on the phase behavior of the blends with TEC plasticizer

By this means, if polyelectrolyte complexes are formed in concentrated polymer solutions or by mixing in a melt, accordingly to the hypothesized model presented in Figure 9, the content of noncovalent crosslinker in a mixture with a film-forming complementary polymer and, consequently, the amount of long chain entanglements, can control the size of loops and free volume. To test this hypothesis, the phase behavior of ternary PDMAEMA-*co*-MMA/BMA blends with a complementary PMAA-*co*-EA noncovalent crosslinker and TEC plasticizer were studied as a function of the PMAA-*co*-EA concentration or polybase–polyacid ratio at a fixed TEC content (45 wt %). Figures 10 and 11 illustrate this relationship.

As is seen from the DSC thermograms shown in Figure 10, under the first scanning, the DSC curves demonstrated endotherms of absorbed water evaporation. Plasticized PDMAEMA-*co*-MMA/BMA contained no water. With the increase of PMAA-*co*-EA content, the amount of absorbed water passed through a maximum (2.5 wt %) in the 1 : 2 blend. The blend of PMAA-*co*-EA polyacid with 45 wt % TEC contained 0.9 wt % water.

In contrast to homogeneous 20 : 1 and 10 : 1 polybase–polyacid blends, all other blends described in this section and containing more polyacid, including also the PMAA-*co*-EA–TEC film, were opaque and implied a two-phase structure of the blends. Besides the PMAA-*co*-EA blend with 45 wt % TEC plasticizer, all of the blends demonstrated, nevertheless,

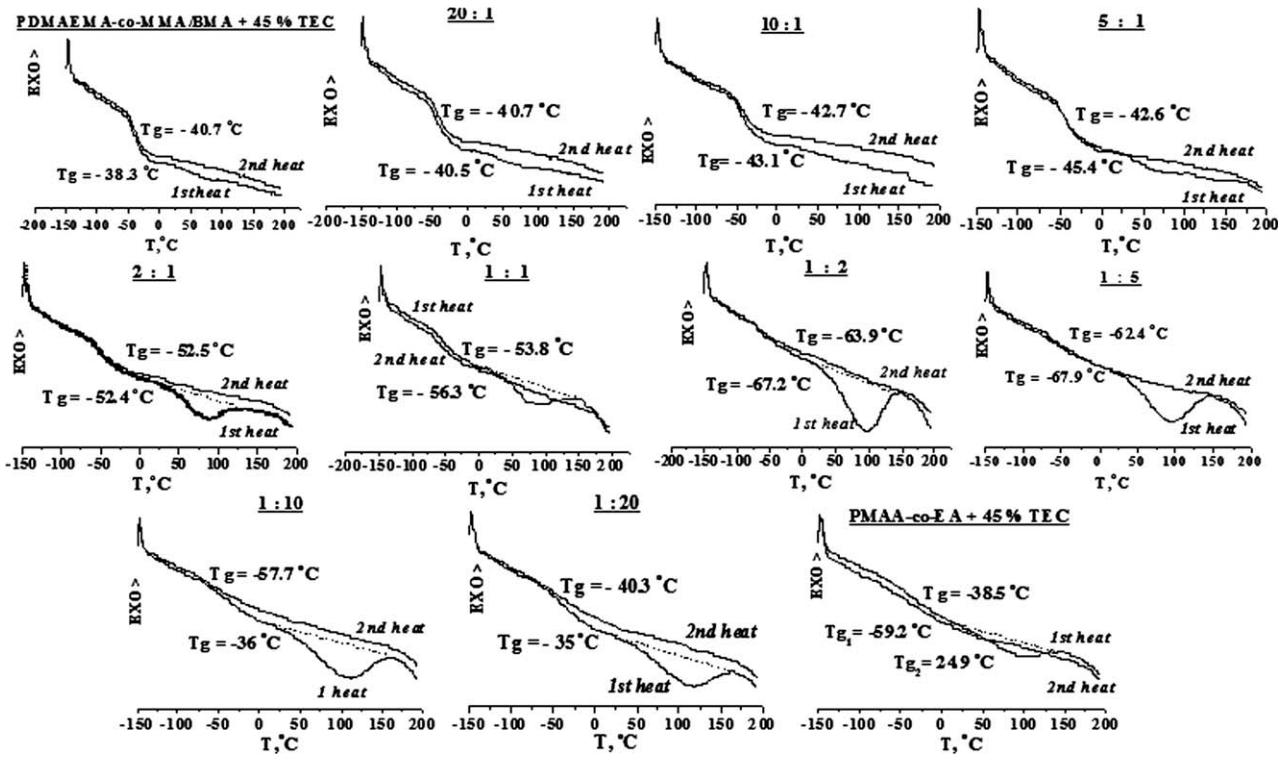

Figure 10 DSC heating thermograms of the binary and ternary blends of polybase and polyacid with 45 wt % TEC plasticizer. The PDMAEMA-*co*-MMA/BMA:PMAA-*co*-EA weight ratio varied from 1 : 0 to 0 : 1 (T = temperature).

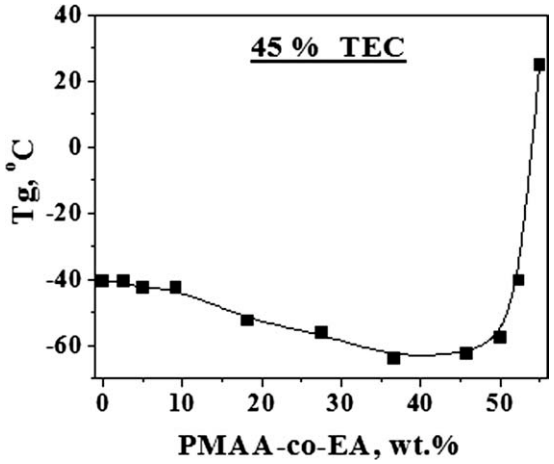

Figure 11 Effect of the PDMAEMA-*co*-MMA/BMA–PMAA-*co*-EA weight ratio on T_g of the polybase–polyacid blends containing 45 wt % TEC plasticizer (data of repeated scanning).

only a single T_g. The occurrence of a single T_g for two-phase polymer blends has been really observed for polymer systems with microphase separation.[55] In such systems, the upper T_g phase is composed of finely divided particles, which are uniformly distributed within a continuous, low-T_g phase. The alternative reason behind single T_g existence in opaque PDMAEMA-*co*-MMA/BMA blends with higher contents of PMAA-*co*-EA and TEC plasticizer could be a compatibilizing effect of the plasticizer.

As is seen from Figure 10, the polyacid mixture with plasticizer displayed a single T_g at −38.5°C in the first scan but two glass transitions at −59.2 and 24.9°C at the repeated heating. The lower T_g in this blend was thought to characterize the TEC-enriched phase, whereas the upper T_g related most likely to the PMAA-*co*-EA enriched phase. Although ΔC_p was very pronounced for the plasticized PDMAEMA-*co*-MMA/BMA polybase (ΔC_p = 0.62 J g^{-1} K^{-1} in the first scan and 0.43 J g^{-1} K^{-1} in the second scan), the glass transitions in the PMAA-*co*-EA–TEC mixture were much less expressed (0.11–0.12 J g^{-1} K^{-1}). In the plasticized blends of the PDMAEMA-*co*-MMA/BMA polybase with the PMAA-*co*-EA polyacid, the ΔC_p decreased smoothly with the rise of the content of noncovalent crosslinker, PMAA-*co*-EA.

As follows from the data in Figure 11, the T_g of the ternary PMAA-*co*-MMA/BMA blends with PMAA-*co*-EA and TEC plasticizer decreased only slightly with the rise of the concentration of noncovalent crosslinker up to 10 wt % of the PMAA-*co*-EA. Mixing with the polyacid resulted in a more pronounced T_g decrease. Within the range of PMAA-*co*-EA concentrations of 36.7–45.8 wt %, the blend's T_g approached a value that was only 5°C higher than that featured for the T_g of unblended TEC and then climbed sharply. In this way, especially large negative T_g deviations from the simple rule of polymer mixing were observed for the blends enriched with noncovalent crosslinker (PMAA-*co*-EA polyacid); this implied an appreciable free volume formation in these blends.

Effect of the polyelectrolyte ionization on the phase behavior of the blends

As was shown in our recent article,[21] the ionization of amino and carboxyl functional groups in the polyelectrolyte blends of the PDMAEMA-*co*-MMA/BMA polybase with the PMAA-*co*-EA polyacid and TEC plasticizer had a dramatic impact on the mechanism of molecular interactions in the blends, as evidenced by IR-Fourier transform spectra. Quantum chemical analysis demonstrated that the energy of ionic and hydrogen bonding diminished in the following order: multicomponent complexes involving protonated amino groups of DMAEMA (ammonium cation) in the presence of chlorine counterion with ionized or unchanged carboxyl groups and water molecules (690–520 kJ/mol) > ternary H-bonded polyelectrolyte complexes associated with molecule of water (520–420 kJ/mol) > binary ionic complex of carboxylate anion and ammonium cation (404 kJ/mol) > H-bonded complex of carboxylate and ammonium ions (257 kJ/mol) > binary H-bonded complex of uncharged carboxyl group with ammonium cation (114 kJ/mol) > ternary H-bonded complex of uncharged carboxyl group, amino group, and water molecule (43 kJ/mol) > binary H-bonded complex between nonionized carboxyl and amino groups (26 kJ/mol). The proton-donating capability of functional groups in the studied polyelectrolyte blends diminished in the following order: $HN^+(CH_3)_2$— > HOOC— > HO—. It could be significantly improved in the presence of Cl^- ions, the effect of which may have been appreciably inhibited when Na^+ cations were available in the blend or solution. The proton-accepting capability weakened in the following order: uncharged amino groups > carboxylate anion > uncharged carboxyl groups > hydroxyl groups in the molecules of TEC plasticizer or absorbed water. Both the large-strain mechanical and adhesive properties of the blends were very strongly affected by the ionization of the polyelectrolyte functional groups in the range of ionization degree from 0 to 20 mol %.[19,20,56] Further ionization did not lead to any more change in the physical properties.

In contrast, as is seen from the data listed in Table II, the protonation of PDMAEMA-*co*-MMA/BMA amino groups and the ionization of PMAA-*co*-EA carboxyl groups in the blends had no appreciable effect on the phase behavior. Only a single glass transition was observed in the blends, the

TABLE II
T_g's and Values of ΔC_p for Partly Ionized Polyelectrolyte Blends Containing 25 wt % of TEC Plasticizer

Ionized component	Ionization degree (mol %)	T_g (°C)	ΔC_p (J $g^{-1}\cdot K^{-1}$)
PDMAEMA-*co*-MMA/BMA	0	−29.0 to −21.3	0.32–0.26
	5	−22.0	0.13
	10	−20.6	0.15
	20	−21.7	0.16
PMAA-*co*-EA	0	−29.0 to −21.3	0.32–0.26
	5	−23.3	0.18
	10	−21.7	0.17

The polybase–polyacid ratio was 10 : 1.

temperature of which was practically invariable with the change of ionization degree of the polyelectrolyte functional groups, which ranged from 0 to 20 mol %. This fact implies that the contribution of the increase in the energy of the intermolecular cohesion to the value of T_g [Eq. (1)] was counterbalanced by the increase of free volume due to the electrostatic repulsion of identical positive or negative charges in the chains of PDMAEMA-*co*-MMA/BMA and PMAA-*co*-EA, respectively.

It is interesting to note that the phase state of the unblended polybase and polyacid was sensitive to the ionization of their functional groups (see Phase State of the Unblended Components section), whereas the blends of complementary polyelectrolytes were much more tolerant. It was apparent that the specific bonding of carboxyl and amino groups made the blends more stable to the change of pH.

Phase state of the unplasticized stoichiometric polyelectrolyte complex

The previously presented data related mainly to the plasticized 20 : 1 and 10 : 1 polybase–polyacid blends, in which nonstoichiometric complexes of so-called scrambled egg structure were typically formed.[57,58] In such polyion complexes, only partial and mainly random charge-compensation occurs, and when complementary polyelectrolytes are mixed in an uncharged state, only comparatively short sequences of interchain H bonds are available. In contrast, as the polybase–polyacid ratio in the blends approached 1, stoichiometric complexes of a ladderlike structure were formed, in which all of the charged units of polyelectrolyte chains were internally compensated by oppositely charged units from the other polyelectrolyte. As a result, the stoichiometric complex exhibited properties that were very distinct from those of the unblended polyelectrolytes. Typically, as the complex formation occurred in a common solvent, a stoichiometric polyelectrolyte complex precipitated; this indicated that it became incompatible both with the parent polyelectrolytes and the solvent. In this section, we consider phase behavior of the inhomogeneous 5 : 1, 2 : 1, and 1 : 1 PDMAEMA-*co*-MMA/BMA – PMAA-*co*-EA blends, prepared by casting–drying from ethanol solutions in the absence of plasticizer. With this purpose, the sol fraction, composed mainly of a scrambled egg polyelectrolyte complex, was separated by filtration from the insoluble gel fraction of a ladderlike complex, and the phase states of both fractions upon drying were characterized separately.

As follows from DSC thermograms presented in Figure 12 and the data listed in Table III, T_g of the ladderlike complex in the gel phase was higher by 30–40°C in the first heating scans and by 50–60°C in the second scans than the T_g values of the scrambled egg complex in the sol fraction. In view of Eq. (1), this was an indication that the density and, consequently, the cohesive strength of the network of noncovalent bonds in the gel phase were significantly higher than in the sol fraction. In other words, the length of the ladderlike network junctions in the stoichiometric complex of the gel phase was much greater.

This conclusion was confirmed with the TEM data presented in Figure 13. As follows from the electron microphotographs shown in this figure, the particles of the 70 : 30 polyelectrolyte complex separated from the sol fraction demonstrated a lamellar structure that is typical of the nonstoichiometric complex of the scrambled egg morphology possessing a large free volume. In contrast, the particles of the 50 : 50 stoichiometric complex formed in the gel phase had a fibrillar network structure, which is more typical of the ladderlike polyelectrolyte complex, wherein intermolecular cohesion energy dominates free volume.

With the increase of the concentration of the noncovalent crosslinker (polyacid) from 5 : 1 to 1 : 1, T_g of gel fraction tended to decrease by approximately 10°C in the first scan and to increase by about the same value in the thermograms of the second heating (Table III). The difference in the results of the two scannings implied most likely that the structure of the ladderlike polyelectrolyte complex was a subject of appreciable relaxation under heating. For the sol fraction, the increase of polyacid concentration resulted in an appreciable decrease of the T_g value (by about 20°C) under the first heating only. In the thermograms of the second scanning, the T_g change could not be reliably established because the DSC thermogram of the 1 : 1 complex demonstrated two T_g values of 40.4 and 79.1°C, correspondingly. It is worth noting that the upper T_g value was close to the value found for the gel fraction (Table III).

The characteristic feature of the DSC thermograms of the gel fractions in the 5 : 1, 2 : 1, and 1 : 1

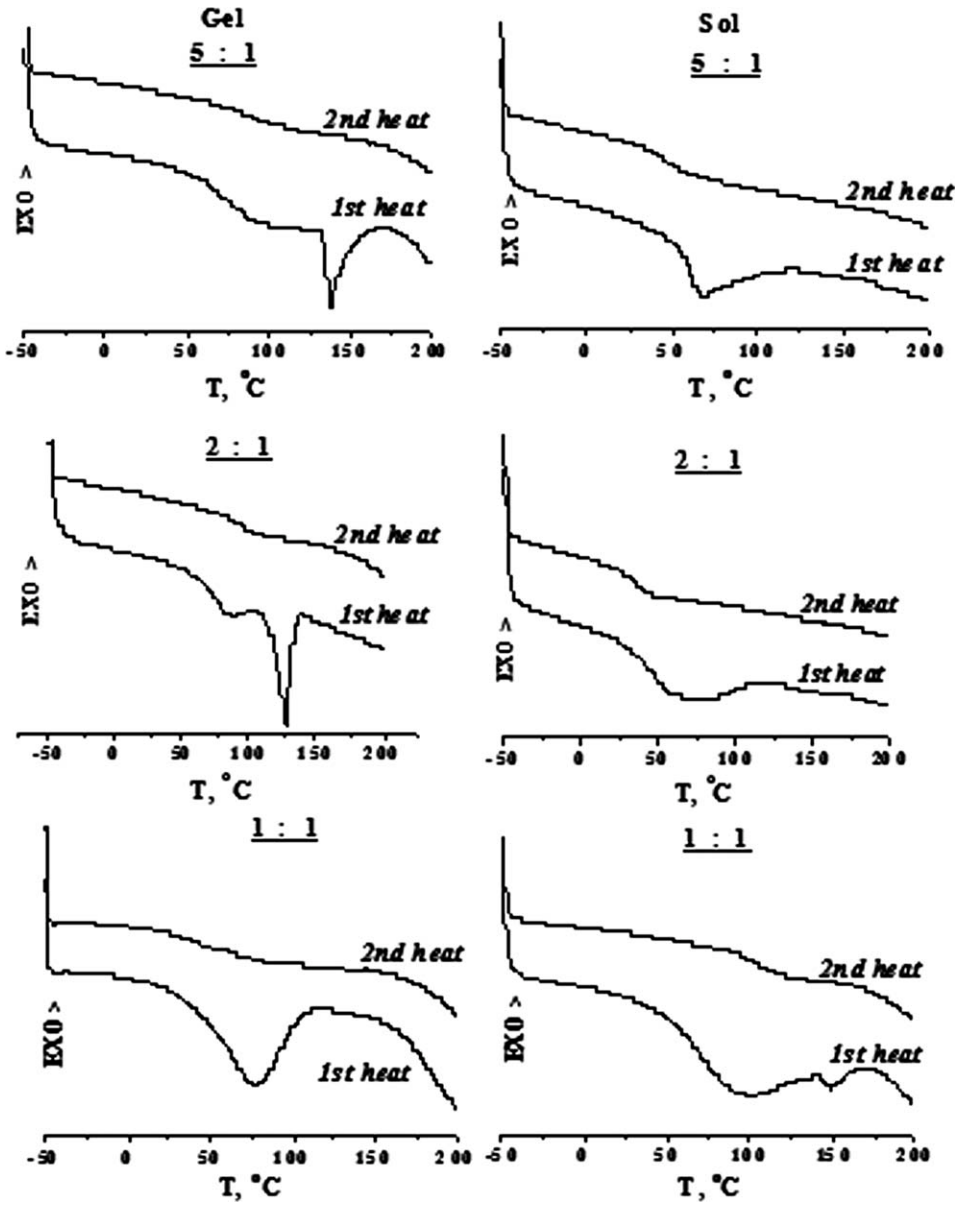

Figure 12 DSC thermograms of unplasticized 5 : 1, 2 : 1, and 1 : 1 PDMAEMA-*co*-MMA/BMA–PMAA-*co*-EA complexes in the gel (left) and sol (right) phases (T = temperature).

polybase–polyacid blends, shown in Figure 12, was the presence of high-temperature endothermic peaks, which resembled the endotherms of melting. These peaks were observed in the thermograms of the first heating only and tended shifting to lower temperatures for the 5 : 1 and 2 : 1 blends compared to the 1 : 1 complex. Although the crystallinity has been really reported for stoichiometric polyelectrolyte complexes of perfect ladderlike structure,[59] this is not the case for the system considered in our study. As the WAXS data in Figure 14 demonstrate, the samples of the polyelectrolyte blends, showing high temperature endotherms in DSC thermograms of the first heating, were fully amorphous. The X-ray diffraction patterns of the gel phase of the 5 : 1 and 2 : 1 polybase–polyacid complexes in Figure 14 exhibit an amorphous halo and the lack of sharp peaks typical for crystalline polymers. The intensities of the highest peaks in Figure 14 are comparable with noise amplitude and show no correlation with sufficiently great changes of enthalpy for the endotherms at 137 and 128°C for the 5 : 1 and 2 : 1 blends in Figure 12 (enthalpy of endotherms (ΔH) = 14 and 20 J/g, respectively). By this means, the most plausible origin of the high-temperature endotherms in Figure 12 was the relaxation of the polyelectrolyte complex structure, which occurred as the intermolecular interactions fell off and the molecular mobility of the polymer chains increased with the elevation in temperature.

TABLE III
Characteristics of DSC Heating Thermograms for the 5 : 1, 2 : 1, and 1 : 1 PDMAEMA-co-MMA/BMA Polybase-PMAA-co-EA Polyacid Complexes Obtained from the Sol and Gel Phases of Ethanol Solution in the Absence of Plasticizer

Polybase–polyacid ratio		First scan				Second scan			
		Glass transition		High-temperature peak		Glass transition		High-temperature peak	
		T_g (°C)	ΔC_p (J/g·K)	T (°C)	ΔH (J/g)	T_g (°C)	ΔC_p (J/g·K)	T (°C)s	ΔH (J/g)
5 : 1	Gel	81.8	0.70	137.0	14.3	92.9	0.38	—	—
	Sol	55.4	0.32	—	—	46.4	0.28	—	—
2 : 1	Gel	75.7	0.62	125.7	19.6	93.7	0.31	—	—
	Sol	47.2	0.51	—	—	35.9	0.35	—	—
1 : 1	Gel	72.1	1.16	—	—	104.2	0.37	—	—
	Sol	35.5	0.28	77.5	42.2	40.4	0.17	—	—
	79.1					0.21			

T = temperature.

It is widely believed that the structure and physical properties of polyelectrolyte complexes are poorly reproducible because of the cooperative mechanism of complex formation, impossibility to provide complex dissociation at high temperatures and a large number of variables that determine complex formation. All of these properties are known to be influenced not only by the relative molecular weights and stereochemical fitting of polyelectrolyte chains, charge densities, and so on but also by secondary experimental conditions such as the concentrations, the order of polyelectrolyte mixing, their mixing ratio, ionic strength, pH, temperature of the solution, and stirring rate. In this connection, it is pertinent to note that experimental conditions of complex preparation, accepted in present research, make quite reproducible (with accuracy of 2–5°C) the T_g's of the complexes of different compositions. This was indirect evidence in favor of the uniformity of the polyelectrolyte blends.

Phase-state diagram of the polybase–polyacid blends

WMI study of polybase–polyacid mixing

The principles underlying the WMI technique have been described in detail elsewhere.[35,40,41] Briefly, this technique uses information provided by evolving interference fringe patterns of light transmitted through a sample whose thickness varies gently along the one axis and whose composition varies perpendicular to that axis. Uniform samples exhibit equally spaced interference fringes perpendicular to the axis of increasing sample thickness, whereas the composition gradients in the perpendicular direction cause sharp bending and crowding of the fringes. When all of the components of the polymer blend are miscible, the composition gradient and fringe density are large at early times, following the initial confrontation at the interface, but later relax to a uniform composition, with an associated parallel fringe pattern. When some of the components are immiscible, however, a sharp phase boundary between the two polymer components will appear.

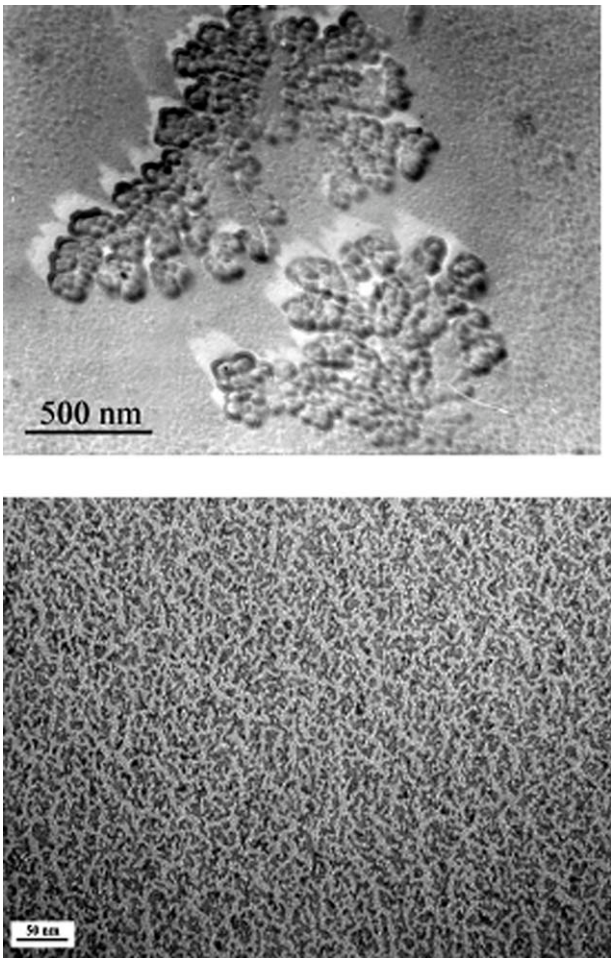

Figure 13 TEM microphotographs of the PDMAEMA-*co*-MMA/BMA–PMAA-*co*-EA complex particles in the sol 70 : 30 (top) and gel 50 : 50 (bottom) phases.

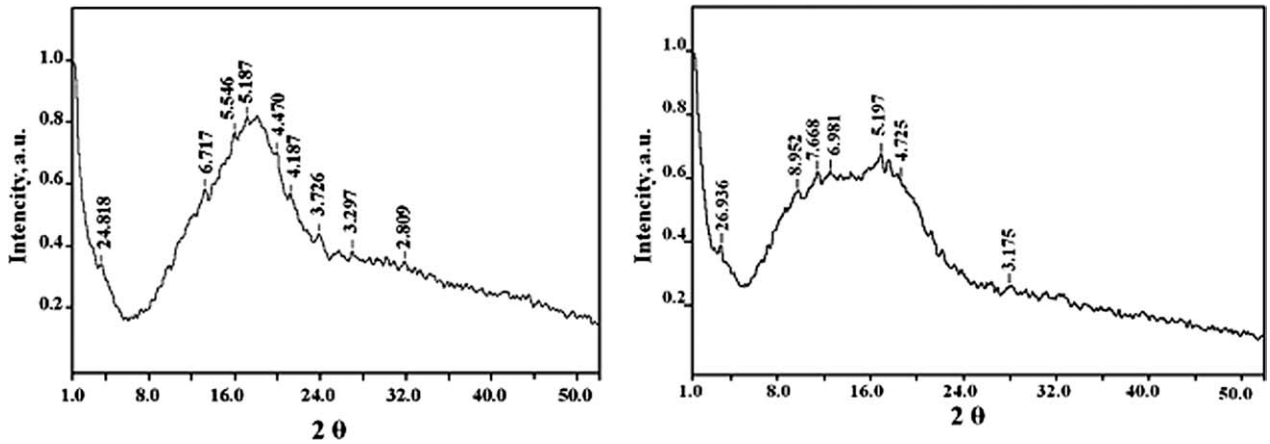

Figure 14 X-ray diffraction patterns of unplasticized 5 : 1 (left) and 2 : 1 (right) PDMAEMA-*co*-MMA/BMA–PMAA-*co*-EA complexes in the gel phase. The relevant interplane distances (Å) are indicated in the figure.

This phase boundary may block light transmission and will show up as a dark band in the interferogram. At equilibrium, parallel fringes are expected on both sides of the interface, but fringe spacings on the two sides will not be the same because of differences in the refractive index. Typical WMI interferograms of the contact interface between the PDMAEMA-*co*-MMA/BMA polybase and PMAA-*co*-EA polyacid at the temperatures above and below complex melting (172°C) are shown in Figure 15. At high temperatures, the interference fringes had a smooth character; this implied gradual changes in the refraction index and blend composition throughout the interdiffusion zone and a transition from one polymer component to another. The width of the transitional zone increased continuously with the rise of observation time. Such interference patterns are typical for miscible polymer systems.

At temperatures below 170°C (Fig. 15, bottom), the interference images demonstrated phase separation and the occurrence of a disperse phase formation along the polybase–polyacid contact interface. This inhomogeneous transitional zone containing inclusions of disperse phase was separated from both parent polymers with distinct phase borders. The width of the transitional zone increased nonlinearly with time, and the moving of the phase boundaries gradually slowed down. Such kinetics of interphase boundary moving was most likely due to the chemical reaction of the polyelectrolyte complex formation rather than the result of interdiffusion of the polybase and polyacid components along the gradient of their concentrations.

Clearly, the particles of the polyelectrolyte complex were immiscible with both parent polymers and formed a separate phase. The interference fringes became straightened, and a jump of the refraction index diminished as a result of the capture of the polybase and polyacid phases with the particles of the formed polyelectrolyte complex. Under elevation of temperatures higher 172°C, the phase boundaries and polyelectrolyte complex particles vanished, and a jump of refraction index arose anew and indicated the reversibility of phase transition due to the melting of the polyelectrolyte complex.

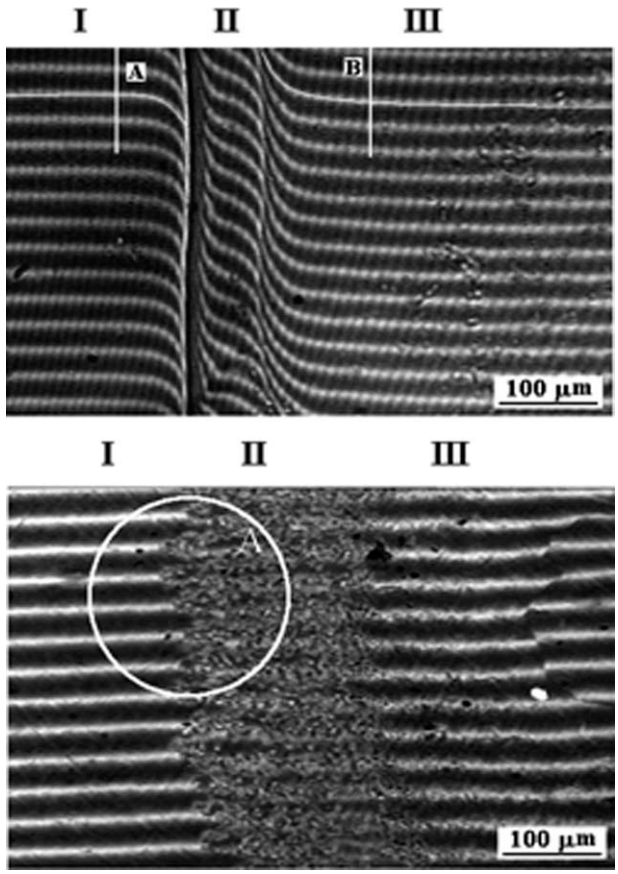

Figure 15 Typical microinterferograms of the contact interface between the PDMAEMA-*co*-BMA/MMA polybase (left) and the PMAA-*co*-EA polyacid (right) at temperatures above 170°C (top) and below 170°C (bottom). (I) PDMAEMA-*co*-MMA/BMA polybase, (II) interdiffusion zone, and (III) PMAA-*co*-EA polyacid. Lines A and B denote the borders of the interdiffusion area. The circle in the bottom interferogram indicates the area observed with the electron microscope (see Fig. 17).

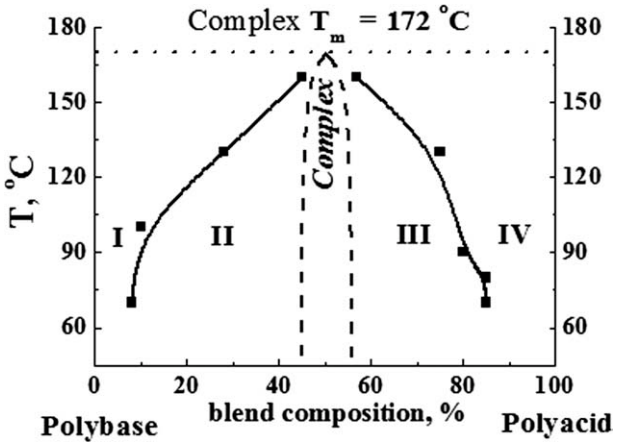

Figure 16 State diagram of the polybase PDMAEMA-*co*-MMA/BMA blends with the PMAA-*co*-EA polyacid. (I) Mixture of the polyelectrolyte complex with the PDMAEMA-*co*-MMA/BMA polybase. (II, III) Nonstoichiometric polybase–polyacid complex and (IV) mixture of the nonstoichiometric complex with PMAA-*co*-EA polyacid. The central zone is occupied by a stoichiometric polyelectrolyte complex of a ladderlike structure (T = temperature; T_m = melting temperature).

Now, let us turn back to the Figure 12 data, where DSC thermograms of the gel fraction revealed the occurrence of high-temperature endotherms that resembled endotherms of melting. Although the WAXS data did not confirm the presence of crystalline phase (Fig. 14), in view of the optical microscopy results obtained in the course of WMI examination (Fig. 15, bottom), which demonstrated the melting of the disperse phase of the stoichiometric polyelectrolyte complex, we can now suppose that the high-temperature endotherm in the DSC scan was due to complex dissociation at high temperatures. Actually, with the rise of temperature, hydrogen bonds between the functional groups in the polybase and polyacid macromolecules became weaker and were eventually destroyed; this resulted in the melting of the disperse phase of the polyelectrolyte complex. The difference in the temperature of the complex melting (172°C in interferograms, shown in Fig. 15, bottom, and 120–150°C in the DSC thermograms, presented in Fig. 12, left) could be explained by the difference in the sample preparation for the WMI and DSC studies. Although the samples of the polyelectrolyte complex for DSC examination formed in solution, those for WMI study were obtained in melt above 172°C followed by cooling.

The characteristic feature of the microinterference images presented in Figure 15 was a splitting of the fringes due to a birefringence effect. The difference in the refraction indices was not so large (0.003–0.004) but was very reproducible. This effect occurs if the structure of a material is anisotropic and implies an ordered structure of the polyelectrolyte complex.

State diagram of the blends of the PDMAEMA-*co*-MMA/BMA polybase with the PMAA-*co*-EA polyacid and supramolecular structure of the solid-state polyelectrolyte complex

On the basis of the WMI data, a phase-state diagram of the PDMAEMA-*co*-MMA/BMA – PMAA-*co*-EA blends was constructed and is presented in Figure 16. In the vicinity of the 1 : 1 polybase–polyacid composition, the blend was characterized by the presence of stoichiometric complex of an ordered ladderlike structure and fibrillar morphology (Fig. 13 bottom) with a melting temperature of about 172°C. To the left and right of the stoichiometric ladderlike polyelectrolyte complex area, the liquidus lines were located, which separated the solid phase of the nonstoichiometric complex from the liquid (molten) phase of the nonstoichiometric complex mixture with parent polymer components. Above the liquidus curve, the area of the homogeneous single-phase blends was located, and below this line, the blends were inhomogeneous two-phase blends. These heterogeneous blends revealed the morphology of a matrix-inclusion type, where the disperse phase was composed of the particles of the polyelectrolyte complex.

To elicit the supramolecular structure of the polyelectrolyte complex formed in the solid state under interfacial polybase–polyacid contact, Figure 17 illustrates the electron microphotograph made within the area under the left branch of the liquidus line of the PDMAEMA-*co*-MMA/BMA–PMAA-*co*-EA state diagram, shown in Figure 16, and within the area denoted by a circle, we present the microinterferogram presented in Figure 15 (bottom). It was evident that the disperse phase particles of the stoichiometric ladderlike polyelectrolyte complex had a fibrillar structure. These particles were incorporated into the

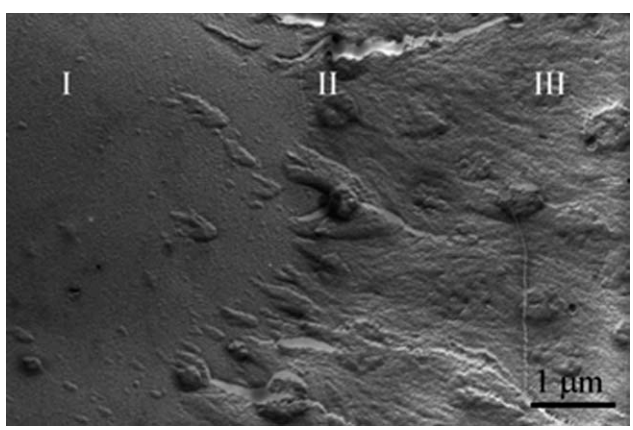

Figure 17 TEM microphotograph of the polyelectrolyte complex supramolecular structure in the area under the left liquidus line: (I) PDMAEMA-*co*-BMA/MMA polybase, (II) interphase contact zone, and (III) stoichiometric polybase–polyacid complex.

continuous PDMAEMA-*co*-MMA/BMA polybase phase, and the border between the phases of the complex and parent polybase was rather nonuniform; this resulted, most likely, from the growth of the ordered complex phase. This behavior was in good accordance with the mechanism presented previously of the polyelectrolyte complex formation.

CONCLUSIONS

The value of T_g is an indicator of the ratio between the energy of intermolecular cohesion and free volume of polymer blends. The growth of cohesion results generally in the increase of T_g value, whereas the rise of free volume leads to the T_g reduction. The blends of the PDMAEMA-*co*-MMA/BMA polybase with the PMAA-*co*-EA polyacid and TEC plasticizer exhibited the occurrence of a single T_g, notwithstanding that only the 20 : 1 and 10 : 1 plasticized polybase–polyacid blends were single phase, whereas the blends of the polybase with higher amounts of the polyacid displayed the signs of microphase separation. The composition behavior of T_g in the PDMAEMA-*co*-MMA/BMA – PMAA-*co*-EA blends with TEC plasticizer demonstrated a predominant contribution of a large free volume formation into the T_g value. Within the framework of a concept of polyelectrolyte complexation, the increase of cohesion was a consequence of the formation of the network of noncovalent interpolymer bonds, whereas the free volume arose as a result of loop formation. It was surmised that polyelectrolyte mixing in the solid state or in concentrated solutions, which led to polymer chain entanglements, favored the formation of the loops of the polymer chains, which were free of intermolecular bonding. The ionization of polyelectrolyte functional groups appreciably affected the phase state of the unblended components but had only an inappreciable impact on the T_g behavior in the polyelectrolyte blends. The measured T_g values were fairly reasonably correlated with earlier established mechanisms of molecular interaction in the PDMAEMA-*co*-MMA/BMA – PMAA-*co*-EA – TEC blends.[21]

The phase state of the polyelectrolyte complexes of a so-called scrambled egg structure in the sol fraction and the ladderlike network complex in the gel fraction were characterized with T_g. The T_g values were always higher for the stoichiometric ladderlike complex than for the nonstoichiometric polyelectrolyte complexes of the scrambled egg structure. This fact was a direct confirmation that the intermolecular cohesion dominated the free volume in the ladderlike complex, whereas in the slightly crosslinked complexes of scrambled egg structure, the free volume due to loop formation dominated the energy of intermolecular cohesion. When the polyelectrolyte complexes were not separated by the filtration of casting solution before dry blend preparation, the scrambled egg complex formed a continuous phase of lower T_g, whereas the finely divided particles of the ladderlike complex in dispersed phase with upper T_g had microscopic sizes and did not show a separate T_g value. The supramolecular structures of the nonstoichiometric and stoichiometric polyelectrolyte complexes were studied with electron microscopy. A nonstoichiometric scrambled egg complex in the sol phase exhibited a lamellar structure, whereas a stoichiometric ladderlike complex in the gel phase formed a well-developed fibrillar network structure that resembled a nanosized web.

A state diagram of the polybase–polyacid blends revealed areas of partial component miscibility and the formation of the complex of the scrambled egg structure, which were separated by a field occupied by the ladderlike polyelectrolyte complex of stoichiometric composition, which was immiscible with both parent polymers at temperatures below 172°C. The melting of the ladderlike complex and polybase–polyacid miscibility above this critical temperature was thought to result from the complex dissociation at high temperatures when intermolecular hydrogen bonds did not exist any longer.

The authors are thankful to Y. M. Korolev and E. M. Antipov for WAXS measurements.

References

1. Van Krevelen, D. W. Properties of Polymers, 3rd ed.; Elsevier: Amsterdam, 1990.
2. Askadskii, A. A. Physical Properties of Polymers: Prediction and Control; Gordon and Breach: Amsterdam, 1996.
3. Bicerano, J. Prediction of Polymer Properties: Marcel Dekker: New York, 1996.
4. Karelson, M. Molecular Descriptors in QSAR/QSPR; Wiley-Interscience: New York, 2000.
5. Todeshini, R.; Consonni, V. Handbook of Molecular Descriptors; Wiley-VCH: Weinheim, 2000.
6. Sun, H.; Tang, Y.; Zhang, F.; Wu, G.; Chan, S.-K. J Polym Sci Part B: Polym Phys 2002, 40, 2164.
7. Yu, X.; Wang, X.; Li, X.; Gao, J.; Wang, H. J Polym Sci Part B: Polym Phys 2006, 44, 409.
8. Sun, H.; Tang, Y.; Wu, G.; Zhang, F. J Polym Sci Part B: Polym Phys 2002, 40, 454.
9. Belfiore, L. A.; Lutz, T. J.; Cheng, C.; Bronnimann, C. E. J Polym Sci Part B: Polym Phys 1990, 28, 1261.
10. Seitz, J. T. J Appl Polym Sci 1993, 49, 1331.
11. Gao, J.; Xu, J.; Chen, B.; Zhang, Q. J Molecular Model 2007, 13, 573.
12. Kuhn, R.; Kroemer, H. Microchim Acta 1991, 104(1–6), 225.
13. Andrews, E. H. Angew Chem 1974, 13, 113.
14. Klun, T. P.; Wendling, L. A.; Van Borgart, J. W. C.; Robbins, A. F. J Polym Sci Part A: Polym Chem 1987, 25, 87.
15. Grigorieva, O.; Slisenko, O.; Bismarck, A.; Sergeeva, L. Macromol Symp 2007, 254, 233.
16. Handbook of Pressure-Sensitive Adhesives and Products; Benedek, I.; Feldstein, M. M., Eds.; CRC/Taylor & Francis: London, 2009; Vols. 1–3.

17. Developments in Pressure-Sensitive Products, 2nd ed.; Feldstein, M. M., Benedek, I., Eds.; CRC/Taylor & Francis: London, 2006; Chapter 4, p 119.
18. Handbook of Pressure-Sensitive Adhesives and Products; Feldstein, M. M., Benedek, I., Eds.; CRC/Taylor & Francis, 2009; Chapter 10, p 10.
19. Feldstein, M. M.; Kireeva, P. E.; Kiseleva, T. I.; Gdalin, B. E.; Novikov, M. B.; Anosova, Y. V.; Shandryuk, G. A.; Singh, P.; Cleary, G. W. Polym Sci Ser A 2009, 51, 799.
20. Feldstein, M. M.; Cleary, G. W.; Singh, P. In Pressure-Sensitive Design and Formulation; Benedek, I., Ed.; VSP: Leiden, The Netherlands, 2006.
21. Feldstein, M. M.; Kiseleva, T. I.; Bondarenko, G. N.; Kostina, J. V.; Singh, P.; Cleary, G. W. J Appl Polym Sci 2009, 112, 1142.
22. Dubin, P.; Bock, J.; Davis, R.; Schulz, D.; Thies, C. Macromolecular Complexes in Chemistry and Biology; Springer: Berlin, 1994.
23. Coleman, M. M.; Graf, J. F.; Painter, P. C. Specific Interactions and the Miscibility of Polymer Blends; Technomic: Lancaster, PA, 1991.
24. Tsuchida, E.; Abe, K. Interaction between Macromolecules in Solution and Intermacromolecular Complexes; Springer-Verlag: Berlin, 1982.
25. Kabanov, V. A.; Zezin, A. B. Pure Appl Chem 1984, 65, 343.
26. Jiang, M.; Li, M.; Xiang, M.; Zhou, H. Adv Polym Sci 1999, 146, 121.
27. Mende, M.; Petzold, G.; Buchhammer, H.-M. Colloid Polym Sci 2002, 280, 342.
28. Zhang, G.; Jiang, M.; Zhu, L.; Wu, C. Polymer 2001, 42, 151.
29. Izumrudov, V. A.; Sybachin, A. V. Polym Sci Ser A 2006, 48, 1098.
30. Kunze, K. K.; Netz, R. R. Europhys Lett 2002, 58, 299.
31. Philippova, O. E.; Khokhlov, A. R. In Polymer Gels and Networks; Osada, Y., Kokhlov, A. R., Eds.; Marcel Dekker: New York, 2001; p 163.
32. Castelnovo, M.; Joanny, J. F. Phase Diagram of Diblock Polyampholyte Solutions, 2001. Cornell University Library. http://arxiv.org/PS_cache/cond-mat/pdf/0112/0112181v1.pdf. date of access Feb., 2008.
33. Kireeva, P. E.; Shandryuk, G. A.; Kostina, J. V.; Bondarenko, G. N.; Singh, P.; Cleary, G. W.; Feldstein, M. M. J Appl Polym Sci 2007, 105, 3017.
34. Kireeva, P. E.; Novikov, M. B.; Singh, P.; Cleary, G. W.; Feldstein, M. M. J Adhes Sci Technol 2007, 21, 531.
35. Bayramov, D. F.; Singh, P.; Cleary, G. W.; Siegel, R. A.; Chalykh, A. E.; Feldstein, M. M. Polym Int 2008, 57, 785.
36. Feldstein, M. M.; Shandryuk, G. A.; Platé, N. A. Polymer 2001, 42, 971.
37. Feldstein, M. M.; Kuptsov, S. A.; Shandryuk, G. A.; Platé, N. A. Polymer 2001, 42, 981.
38. Feldstein, M. M.; Roos, A.; Chevallier, C.; Creton, C.; Dormidontova, E. D. Polymer 2003, 44, 1819.
39. Chalykh, A. E.; Gerasimov, V. K.; Mikhailov, Y. M. Phase Diagrams of Polymer Systems; Yanus-K: Moscow, 1998.
40. Bairamov, D. F.; Chalykh, A. E.; Feldstein, M. M.; Siegel, R. A.; Platé, N. A. J Appl Polym Sci 2002, 85, 1128.
41. Bairamov, D. F.; Chalykh, A. E.; Feldstein, M. M.; Siegel, R. A. Macromol Chem Phys 2002, 203, 2674.
42. Novikov, M. B.; Roos, A.; Creton, C.; Feldstein, M. M. Polymer 2003, 44, 3559.
43. Fox, T. G. Bull Am Phys Soc 1956, 1, 123.
44. Gordon, M.; Taylor, J. S. J Appl Chem 1952, 2, 493.
45. Kwei, T. K. J Polym Sci Polym Lett 1984, 22, 307.
46. Lu, X.; Weiss, R. A. Macromolecules 1992, 25, 3242.
47. Song, M.; Hourston, D. J.; Pollock, H. M.; Hammiche, A. Polymer 1999, 40, 4763.
48. Slark, A. T. Polymer 1997, 38, 2407.
49. Kwei, T. K.; Pearce, E. M.; Pennachia, J. R.; Charton, M. R. Macromolecules 1987, 20, 1174.
50. Saeki, S.; Cowie, J. M. G.; McEven, I. J. Polymer 1983, 24, 60.
51. Feldstein, M. M. Polymer 2001, 42, 7719.
52. Schneider, H. A. Polymer 1989, 30, 771.
53. Zezin, A. B.; Rogacheva, V. B. In Advances in Physics and Chemistry of Polymers; Berlin, A. A., Kabanov, V. A., Rogovin, Z., Slonimskii, G. L., Eds.; Khimiya: Moscow, 1973; p. 3.
54. Petrak, K. J Bioact Compat Polym 1986, 1, 202.
55. Bershtein, V. A.; Egorov, V. M. Differential Scanning Calorimetry of Polymers: Physics, Chemistry, Analysis, Technology; Ellis Horwood: New York, 1994; p 272.
56. Feldstein, M. M.; Cleary, G. W.; Singh, P. In Technology of Pressure-Sensitive Adhesives and Products; Benedek, I., Feldstein, M. M., Eds.; CRC/Taylor & Francis: London, 2009; Chapter 7, p. 7.
57. Thünemann, A. F.; Müller, M.; Dautzenberg, H.; Joanny, J.-F.; Löwen, H. Adv Polym Sci 2004, 166, 113.
58. Michaels, A. S. Ind Eng Chem 1965, 57(10), 32.
59. Kabanov, V. A. Russ Rev Chem 2005, 74, 3.